Microfluid Nanofluid (2011) 10:337–353
DOI 10.1007/s10404-010-0672-6

RESEARCH PAPER

Roles of solution conductivity mismatch in transient current and fluid transport in electrolyte displacement by electro-osmotic flow

Szu-Wei Tang · Chien-Hsiang Chang · Hsien-Hung Wei

Received: 21 April 2010 / Accepted: 4 July 2010 / Published online: 22 July 2010

Abstract Electro-osmotically driven displacement between two solutions having a conductivity mismatch is theoretically examined. Internal pressures induced by the conductivity mismatch can affect the propagation of the solution interface and the behavior of the transient current. Combining Ohm's law and fluid mass conservation, we derive a coupled set of length-averaged equations accounting for how the electric current and the traveling distance of the solution interface vary with time, electric field, and the solution conductivities. Extension to successive displacements involving multiple solution zones is made to reveal non-monotonic and stagewise changes in transient currents. For the first time, critical roles of surface conductance on displacements in highly charged channels are unraveled. We show that if the lower conductivity solution has a greater valence than the higher one, the effective conductivity of the former can exceed that of the latter when the channel height is below some critical value. The resulting transient current behavior can turn opposite to that usually observed in the large-channel case, offering a new paradigm for gauging the importance of surface conductance in submicron charged channels. Possible impacts of diffusion smearing and hydrodynamic dispersion are also discussed by including the additional mixing zone into the analysis. Having shown good agreement with the existing experimental data, our analysis not only captures the natures of solution displacement by electro-osmotic flow (EOF), but also extends the applicability of the current monitoring method for measuring surface zeta potentials of microchannels.

S.-W. Tang · C.-H. Chang · H.-H. Wei (✉)
Department of Chemical Engineering, National Cheng Kung University, Tainan 701, Taiwan
e-mail: hhwei@mail.ncku.edu.tw

Keywords Electro-osmotic flow · Solution displacement · Solution conductivity mismatch · Transient current · Surface conductance · Current monitoring method

1 Introduction

Electro-osmotic flow (EOF) is the motion of an electrolyte solution over a charged surface under the actions of an applied electric field. The origin of this phenomenon lies in the existence of the thin electric double layer of 1–100 nm in thickness adjacent to the surface. This layer, in order to neutralize the proximate surface charge, acquires excess counterions from the bulk, behaving like a mobile charge sheath near the surface. When an electric field E is applied, it imparts an electric force to drive the fluid therein, dragging the adjacent bulk along with it. In a macroscopic point of view, the phenomenon would look like as if the surface were sliding. This is EOF with the apparent slip velocity U characterized by the well-known Smoluchowski formula (Probstein 1994):

$$U = -\frac{\varepsilon\zeta E}{\eta}, \tag{1}$$

where ε and η are the permittivity and viscosity of the electrolyte solution, respectively, and ζ is the zeta potential of the surface.

As illustrated in Fig. 1, this study is motivated by the use of EOF in displacing one solution by another with a conductivity difference for measuring the surface zeta potential of a uniformly charged channel (Huang et al. 1988; Ren et al. 2002; Sze et al. 2003). If the conductivity difference is small, the interface between the solutions can be kept flat by a nearly uniform flow and progress at a

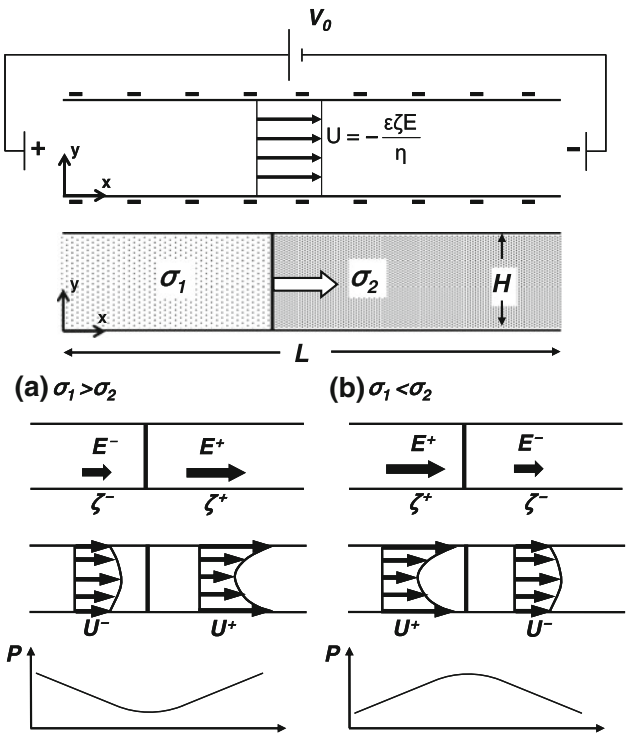

Fig. 1 Schematic illustration showing how a solution conductivity difference influences the electric field (E), zeta potential (ζ), EOF slip velocity (U), and fluid pressure (P) during an EOF-driven displacement in a uniformly charged microchannel. **a** Illustrates the situation when a higher conductivity solution displaces a lower one ($\sigma_1 > \sigma_2$), and **b** corresponds to that when a lower conductivity solution displaces a higher one ($\sigma_1 < \sigma_2$)

constant speed according to Eq. 1. This uniform sweeping leads the partition between the solutions to vary at a constant rate, giving a steady change in the electric resistance over the channel. As the resulting electric current varies linearly with time at the rate proportional to the displacement speed, the surface zeta potential of the channel can be readily determined by tracking the linear change in the transient current during the displacement. This method has been recently extended to measure the surface zeta potentials of a composite microchannel (Kuo et al. 2008).

However, solution conductivity difference can cause two effects. First, the electric fields in the solutions are not equal, as required by Ohm's law which states that electric current density must remain constant throughout the channel. Second, because surface zeta potential varies inversely with solution conductivity (Kirby and Hasselbrink 2004), it can have different values in the solutions. These two effects combined lead to unequal EOF velocities in the solutions. But fluid mass conservation entails that additional pressures must be developed for assisting or opposing the EOFs for maintaining a constant flow rate across the channel depth. Such pressure flows can lead the displacement speed to vary with position along the channel, making the transient current no longer changed at a constant rate. If this internal pressure effect were not properly taken into account, there could be an inaccuracy in the zeta potential measurement. It is therefore necessary to quantify how the transient current and the displacement speed are influenced by these effects due to the conductivity mismatch, which is the main theme of this article.

There are a number of studies on EOF-driven solution displacement. Li and his coworkers considered an electrolyte replacing process in a cylindrical microcapillary (Arulanandam and Li 2000; Ren et al. 2002). They solved the Poisson equation and the equation of motion to find the electric potential distribution and the EOF velocity profile in the radial direction of the capillary. The averaged flow speed was then determined as functions of the zeta potential, electric field, and the properties of the fluid. This approach is essentially the same as that for deriving the Smoluchowski formula. Monitoring the current changes in these studies was merely used to find the displacement time for determining the averaged flow speed, which is in the same spirit as that of Huang et al. (1988). Ren et al. (2001) later coupled the Poisson equation, the convection–diffusion equation, and the Navier–Stokes equation to account for interplay between the concentration distribution, the electric potential distribution, and the fluid motion. Solving these equations numerically, they were able to capture the successive change in the transient current and found it in good agreement with that measured by experiment. The similar approach was also employed to study solution displacement in a rectangular microchannel (Wang et al. 2007). In the study by Ren et al. (2003), an equivalent circuit model was developed to elicit how the traveling distance of the solution interface depends on the transient current and the solution conductivities. Recently, a modified circuit model has also been proposed to characterize the transient current behavior during a displacement in a composite microchannel in which the solution interface is advected obliquely by a linear EOF (Kuo et al. 2008).

While these previous studies did reveal some features of solution displacement process, we feel that the roles of solution conductivity difference in affecting the natures of the displacement are somewhat less clear. For those using the Smoluchowski-like approach (Arulanandam and Li 2000; Ren et al. 2002), the surface zeta potential was assumed uniform everywhere—its difference in the two solutions was not taken into account. In full numerical studies (Ren et al. 2001; Wang et al. 2007), although the models thereof are sophisticated enough to capture all the relevant effects, one must rely on extensive simulations to reveal the features of the systems; this approach cannot tell explicitly how the current changes and how fast the solution interface travels during the process. The circuit model did reveal how the extent of the displacement depends on the transient current and the solution conductivities

(Ren et al. 2003). And yet, the influence of the induced pressure flow on the interface movement was not brought out, though it did contribute to part of the result.

In this work, we would like to complement previous studies by clarifying the roles of solution conductivity difference in EOF-driven solution displacement. In particular, we would like to look at potential impacts on the current monitoring method for measuring surface zeta potentials. Our aim is to develop a simple analytical approach for revealing essential physics of the displacement. To do so, we take advantage of the fact that the double layer is much thinner than the channel depth, so that electrostatic body forces within the double layer are simply transmitted into the slip velocity to drive the bulk flow outside the double layer, rendering the well-known Smoluchowski formula as the *effective* boundary condition to drive the bulk flow. In addition, because of the persisted Poisson–Boltzmann equilibrium across the double layer, electroneutrality can be maintained in most portions of the fluid. Consequently, the solutions are always sweeping at the respective Smoluchowski slip velocities over the surface and the electrolyte concentration remains virtually unchanged across the channel depth. This simplification not only enables us to take a global balance for the electric current (i.e., Ohm's law), but also allows us to analyze the fluid transport without having to resolve the ion concentration distribution in detail. That is, in addition to the equation governing the electric flow for maintaining electroneutrality, there will be an analogous equation that takes into account internal pressure effects to describe how the solution interface propagates according to fluid mass conservation. Such an approach has been widely used in analyzing various EOF systems, including EOF in channels with non-uniform zeta potentials or/and varying cross sections (Herr et al. 2000; Ghosal 2002; Brotherton and Davis 2004), sample stacking processes (Chien and Burgi 1992, Devasenathipathy et al. 2007), and electro-osmotic pumping (Chien and Bousse 2002; Takamura et al. 2003).

The article is organized as follows. In Sect. 2, we will scrutinize both the electric flow and the fluid transport problems, and derive a coupled set of equations for the transient current and the traveling distance of the solution interface to elucidate the natures of the displacement. An alternative but much simpler way to derive the equation governing the motion of the solution interface will also be given based on the electrics-hydrodynamics similitude. In Sect. 3, we apply the derived equations to quantify how the transient current and the position of the solution interface vary with time and the solution conductivities. Section 4 is to extend the present framework to successive displacements involving multiple solution zones for illuminating piecewise changes in transient currents. In Sect. 5, we put forth to explore effects of surface conductance. The result will be highlighted by the current flipping phenomenon when displacing polyvalent electrolytes in highly charged channels. Possible impacts from diffusion smearing and hydrodynamic dispersion will be discussed in Sect. 6. In Sect. 7, we discuss the applicability of our analysis and compare our results with the existing experimental data. The article is finally concluded in Sect. 8.

2 Electric flow and fluid transport

As depicted in Fig. 1, consider a solution displacement involving two solutions of different conductivities in a uniformly charged channel of length L and height H. The process begins with one solution of conductivity σ_2 filled in the entire channel. Upon an EOF being set off by a voltage V_0, the other solution of conductivity σ_1 then enters the channel to push the solution ahead of it. This displacement process can be carried out by either displacing the lower conductivity solution with the higher one or another way around, as illustrated, respectively, in Figs. 1a and b.

Suppose that the displacement is sufficiently fast. So the interface can be thought of as a sharp front sweeping through the channel without being significantly smeared by diffusion. Specifically, the condition for neglecting diffusion can be realized if the broadening extent of the solution interface, b, due to diffusion is much smaller than the length of the channel during the displacement time $\tau \sim L/U : b \sim (D\tau)^{1/2} \ll L$ or $b/L \sim Pe_L{}^{-1/2} \ll 1$, where $Pe_L = UL/D$ is the axial Peclet number with U being the scale of the displacement speed and D the ionic diffusivity. We further make a supposition that the interface is flat and advected by the local plug flow therein. Below, we will make use of this local plug flow picture to derive equations governing the electric flow and fluid transport during the displacement. This supposition will be justified a posteriori.

For the electric flow, we demand a constant current density across the channel depth for assuring no net charge accumulation everywhere in the bulk (except for thin electric double layers near the channel walls):

$$\sigma_1 E_1(t) = \sigma_2 E_2(t) = I(t), \tag{2}$$

where E_1 and E_2 are the respective electric fields in the displacing phase and the displaced phase. Let x_f be the traveling distance of the solution interface. Because the potential drop over the channel is $\Delta V_1 + \Delta V_2 = V_0$ with $\Delta V_1 = E_1 x_f$ and $\Delta V_2 = E_2(L - x_f)$, the apparent electric field $E_0 \equiv V_0/L$ turns out to be the length average of the electric fields in the two solutions:

$$\left(\frac{x_f}{L}\right)E_1 + \left(1 - \frac{x_f}{L}\right)E_2 = E_0. \tag{3}$$

Combining Eqs. 2 and 3 yields the well-known Ohm's law: $I = V_0/R$. Here, the overall resistance R over the channel

can be viewed as the two bulk resistors in series: $R = R_1 + R_2$ with $R_1 = x_f/\sigma_1$ and $R_2 = (L - x_f)/\sigma_2$. It can again be re-written in the length-averaged form:

$$R = \left(\frac{x_f}{L}\right)R_{1L} + \left(1 - \frac{x_f}{L}\right)R_{2L}, \tag{4}$$

where $R_{iL} = L/\sigma_i$ is the resistance when the channel is completely filled with solution i. Applying Ohm's law, we arrive at the following equation determining the transient current during the displacement:

$$\frac{I}{I_2} = \frac{1}{1 + (\gamma - 1)\left(\frac{x_f}{L}\right)}, \tag{5}$$

where $I_2 = \sigma_2 V_0/L$ is the current before the displacement and $\gamma = \sigma_2/\sigma_1$ is the conductivity ratio.

Now, we consider the flow problem. The EOF slip velocities in the solutions are given by

$$U_1(t) = v_1 E_1 \quad \text{and} \quad U_2(t) = v_2 E_2, \tag{6}$$

where $v_i \equiv -\varepsilon\zeta_i/\eta$ is the EOF mobility for each phase and generally a decreasing function of σ_i ($i = 1, 2$). Replacing $E_i = I(t)/\sigma_i$ according to Ohm's law, the EOF slip velocity can be re-written as $U_i = v_i I/\sigma_i$. The velocity ratio $U_1/U_2 = \beta\gamma$ can therefore be expressed in terms of the mobility ratio $\beta = v_1/v_2 = \zeta_1/\zeta_2$ and the conductivity ratio $\gamma = \sigma_2/\sigma_1$ ($=(\lambda_1/\lambda_2)^2$ with λ_i being the double layer thickness of solution i). According to the Gouy–Chapman theory, how the zeta potential varies with the double layer thickness is given by $\sinh(ze\zeta/2k_B\widehat{T}) = ze\lambda E_s/2k_B\widehat{T}$ (Hunter 1992), where $E_s = q_s/\varepsilon$ is the surface field arising from the surface charge density q_s, $k_B\widehat{T}/e$ (=25 mV) the thermal energy per unit charge, and z the valence of the electrolyte (which is assumed of symmetric type). For low zeta potential $|\zeta| \ll k_B\widehat{T}/ze$, the linear dependence of the zeta potential on the double layer thickness $\zeta \approx \lambda E_s \propto \sigma^{-1/2}$ leads to $\beta = \gamma^{1/2}$ and $U_1/U_2 = \gamma^{3/2}$. On the other hand, for high zeta potential $|\zeta| > k_B\widehat{T}/ze$, the dependence of the zeta potential on the double layer thickness turns to be $|\zeta| \approx (k_B\widehat{T}/ze)\ \ln(\lambda ze\,|\,E_s\,|\,/k_B\widehat{T})$. Since $\zeta_1/\zeta_2 = 1 + \ln(\gamma^{1/2})/\ln(\lambda_2 ze\,|\,E_s\,|\,/k_B\widehat{T})$ or $1/[1 - \ln(\gamma^{1/2})/\ln(\lambda_1 ze\,|\,E_s\,|\,/k_B\widehat{T})]^{-1}$, we can say $\beta \approx 1$ and $U_1/U_2 \approx \gamma$ if $\ln(\lambda ze\,|\,E_s\,|\,/k_B\widehat{T})$ is much larger than $|\ln(\gamma)|/2$. This scenario is valid if the surface is highly charged and the conductivity difference is not too great. In either limit, the EOF slip velocity is faster (slower) in a lower (higher) conductivity solution. As these two limits suggest that ζ varies with powers between $-1/2$ and 0 in σ, we assume that the dependence of the mobility ratio on the conductivity ratio follows a power law: $\beta = \gamma^{n-1}$ with $1 \le n \le 3/2$, and so the velocity ratio $U_1/U_2 = \gamma^n$.

As required by fluid mass conservation, such a slip velocity difference must induce a forward (backward) pressure flow in the higher (lower) conductivity region to compensate (offset) the lower (higher) flow rate created by the EOFs. Below we analyze the flow field by including the induced pressure flow and then apply it together with Eq. 4 to determine the transient current during the displacement.

Since the flow is unidirectional, the horizontal velocity u in either solution region can be determined by the equation of motion through the balance between the induced pressure gradient and the viscous stress:

$$0 = -\frac{\partial P}{\partial x} + \eta\frac{\partial^2 u_i}{\partial y^2}, \tag{7}$$

subject to boundary conditions $u_i(y = 0) = u_i(y = H) = U_i(t)$. The solution is given by

$$u_i = \frac{1}{2\eta}\frac{\partial P}{\partial x}\left(y^2 - yH\right) + U_i, \tag{8}$$

The flow rate (per unit length) across the channel depth is

$$Q = \int_0^H u_i \mathrm{d}y = -\frac{H^3}{12\eta}\frac{\partial P}{\partial x} + HU_i. \tag{9}$$

This constant flow rate condition is used to determine the pressure distribution in each solution region, yielding

$$P_1(x) = P(x = 0) + \frac{12\eta}{H^3}(U_1 H - Q)x, \tag{10a}$$

$$P_2(x) = P(x = L) + \frac{12\eta}{H^3}(U_2 H - Q)(x - L). \tag{10b}$$

In the case of displacing the lower conductivity solution, because $U_2/U_1 > 1$, the induced pressure flow must be forward ($Q > U_1 H$) in the displacing phase and backward ($Q < U_2 H$) in the displaced phase in order to maintain a constant flow rate across the channel depth. As a result, the pressure must drop in the displacing phase, reach a minimum at the solution interface, and then rise in the displaced phase. Similarly, for displacing the higher conductivity solution, there will be a pressure maximum at the interface. Note that there exists a hydrodynamic transition zone near the interface, which allows the parabolic velocity profile in one phase to gradually evolve into that in the other. Therefore, the flow in the transition zone is not unidirectional (but it does not re-circulate—re-circulation appears when looking at the system in the frame moving with the interface). The situation here is quite similar to the usual entrance flow problem, but the difference is that the transition zone moves along with the interface. The width of the transition zone can be estimated as $\sim H \cdot Re$ (Deen 1998), where $Re = \rho UH/\eta$ is the Reynolds number of the flow with ρ being the density of the fluid. Because Re is typically small, the transition zone actually merely occupies a small fraction of the channel, i.e., $H \cdot Re \ll L$. In other words, the non-parallel flow near the interface is merely confined

within the very narrow transition zone. Therefore, for places sufficiently away from the transition zone, the flow field is fully developed and unidirectional, as considered in the present analysis. If looking at the flow behavior over a large length scale without seeing the detailed flow in the narrow transition zone near the interface, we can say that the flow is unidirectional in most of the channel. And this not only allows us to simplify the problem, but also aids in revealing physics underlying the displacement.

Neglecting the transition zone, the two pressures must match at the interface, $x = x_f(t)$. In addition, the end pressures must be equal, viz., $P(x = 0) = P(x = L)$; otherwise there will be a net flow in the absence of electric fields. Applying these two conditions to Eqs. 10a and 10b, we find

$$Q = x_f\left(\frac{H}{L}\right)(U_1 - U_2) + U_2 H. \tag{11}$$

Fluid mass conservation further entails that the solution interface must travel at the mean velocity of the flow:

$$\frac{\mathrm{d}x_f}{\mathrm{d}t} = \bar{U} \equiv \frac{Q}{H}. \tag{12}$$

Substitution of Eq. 12 into Eq. 11, we arrive at the following equation governing the propagation of the solution interface:

$$\frac{\mathrm{d}x_f}{\mathrm{d}t} = \left(\frac{x_f}{L}\right)U_1 + \left(1 - \frac{x_f}{L}\right)U_2, \tag{13}$$

indicating that the displacement speed is essentially the length average of the two slip velocities according to the extent of the displacement. Note that the form of Eq. 13 for the displacement speed is identical to that of Eq. 3 for the apparent electric field. This is not coincident in view of the fact that both electric field and fluid flow are divergence-free—there is an analogy between electrics and hydrodynamics. In fact, this electrics–hydrodynamics similitude actually offers a simpler way to derive Eq. 13 without having to solve the flow field. In the analogy to Ohm's law for electric flow, the flow rate driven by a pressure ΔP over length L' is $Q_p = \Delta P/(L'/K)$ where L'/K is the flow resistance, and K can be thought of as the mobility of the fluid similar to the role of conductivity in electric flow. Combining the flow rate from the EOF, we can establish a relationship between the total flow rate and the pressure drop for each solution region: $Q = U_i H + K\Delta P_i/L_i$ ($i = 1$, 2). Written in terms of the mean flow velocity that must be equal for both solution regions, it reads $\bar{U} = k\Delta P_1/x_f + U_1 = k\Delta P_2/(L - x_f) + U_2$, where $k = K/H$. Since there is no net pressure across the channel $\Delta P_1 + \Delta P_2 = 0$, this condition together with the above velocity–pressure relationship yields $\bar{U}L = x_f U_1 + (L - x_f)U_2$, which is Eq. 13.

We now make use of Eqs. 2 and 5 to write Eq. 13 in terms of $I(t)$:

$$\frac{\mathrm{d}x_f}{\mathrm{d}t} = U_{20}\left[1 + (\beta\gamma - 1)\left(\frac{x_f}{L}\right)\right]\left(\frac{I}{I_2}\right), \tag{14}$$

where $U_{20} = v_2 E_0$ is the EOF velocity when the channel is completely filled with the displaced phase.

Equation 14 suggests that the movement of the interface can be characterized by different velocity scales, depending on γ. For $\gamma \ll 1$, the characteristic velocity is $U_{20}\, I/I_2 = U_2$, and hence the interface is led by the lower conductivity displaced phase. Similarly, for $\gamma \gg 1$ the interface is pushed by the lower conductivity displacing phase with the velocity scale $U_{20}\,\beta\gamma\, I/I_2 = U_1$. In other words, the fluid motion is controlled by the solution with the faster EOF slip velocity. Alternatively, because $U_2/U_1 = \gamma^{-n}$ (with $n = 3/2$ for low zeta potential or $n = 1$ for high zeta potential), the interface is advected primarily by the lower conductivity solution, as can be seen more directly from Eq. 13. This is actually similar to the fact that the electric flow is dictated by the lower conductivity solution (cf. Eq. 4), as borne out by the electrics–hydrodynamics analogy.

Finally, we would like to justify the locally uniform displacement supposition made in the beginning of this section. This supposition involves two assumptions: (i) the solution interface is flat and remains sharp, and (ii) the interface is advected by a plug flow at the mean flow velocity. However, one might think that the interface could be distorted by the induced pressure flow to one way or the other on either side of the interface. It is not obvious that the interface must travel according to the ways assumed above. Below, we argue that such a locally uniform sweeping is actually the only physically allowable way to advance the interface.

At the interface, the pressure reaches a maximum/minimum at which the pressure gradient vanishes (within the narrow transition region). So there is no curvature for the local velocity profile. As the flow field is symmetric with respect to the centreline, the only admissible velocity profile across the front is uniform. In other words, despite the existence of the induced pressure flow, the flow field at the interface's position is *locally* uniform (but can vary with time). It follows that the interface will always remain flat when it starts, and will travel at the mean flow velocity given by Eq. 12. This also justifies the use of Eq. 2 for the electric flow.

As such, Eqs. 5 and 14 constitute a coupled set of equations for the electric current and the traveling distance of the solution interface. Although a similar set of equations have been derived previously, the efforts were merely focused on modeling sample stacking processes (Chien and Burgi 1992; Devasenathipathy et al. 2007). Here, we derive

these equations for revealing explicitly how solution conductivity difference comes into play in the displacement. Below, we will apply them to quantify how the transient current and the traveling distance of the solution interface vary with time, electric field, and the solution conductivities.

3 Analytical solution and asymptotic results

In this section, we seek the solution for Eqs. 5 and 14. Let $X = x_f/L$, $J = I/I_2$, and $T = t/\tau$ with $\tau = L/U_{20}$ being the characteristic flow time scale based on the velocity in the displaced phase. Then Eqs. 5 and 14 can be re-written in the dimensionless form:

$$J = \frac{1}{1 + \alpha X}, \tag{15}$$

$$\frac{dX}{dT} = (1 + \omega X)J, \tag{16}$$

where $\alpha = \gamma - 1$ and $\omega = \beta\gamma - 1 = \gamma^n - 1$ measure the relative difference between the resistances and that between the velocities of the two solutions, respectively. Note that in the special case of $n = 1$ (in the high zeta potential regime), we have $\beta = 1$ and $\alpha = \omega$, and hence $dX/dT = 1$ from Eqs. 15 and 16. In this case, the displacement speed will always maintain a constant regardless of γ.

Substituting Eq. 15 into Eq. 16 and integrating it with $X(T = 0) = 0$, we find

$$\left(1 - \frac{\alpha}{\omega}\right)\ln(1 + \omega X) + \alpha X = \omega T. \tag{17}$$

Writing Eq. 17 in terms of J with Eq. 15, we can also obtain the solution for J:

$$\left(1 - \frac{\alpha}{\omega}\right)\ln\left(1 + \frac{\omega}{\alpha}(J^{-1} - 1)\right) + J^{-1} - 1 = \omega T. \tag{18}$$

Solving for X and J from Eqs. 17 and 18, the displacement speed can be readily evaluated using Eq. 16. Here, we retain α and ω without writing them in terms of γ in order to distinguish their respective contributions in determining the behavior of the solution. As such, with the aid of Eqs. 17 and 18, for given γ, we are able to reveal quantitatively how both J and X vary with time.

To illuminate how solution conductivity difference influences the natures of the displacement, we asymptotically examine three different cases: (i) $\gamma \approx 1$ when the two solutions' conductivities are nearly matched, (ii) $\gamma \ll 1$ for the displacement by a very high conductivity solution, and (iii) $\gamma \gg 1$ for the use of a very low conductivity solution in advancing the displacement. Note here that we vary γ via changing σ_1 while keeping σ_2 fixed.

3.1 Case (i): $\gamma \approx 1$

Since the zeta potential here is nearly constant ($\beta \approx 1$), all the logarithm terms are dropped out in Eqs. 17 and 18. We recover the usual results for the uniform displacement scenario:

$$J \approx (1 + (\gamma - 1)T)^{-1}, \tag{19}$$

$$X \approx T, \tag{20}$$

Note that in Eq. 19, the $(\gamma - 1)$ term has to be retained to capture the current change arising from the conductivity difference. Equation 19 indicates that the resistance ($\propto J^{-1}$) varies linearly with time. This is evident, since the interface travels at a constant speed in a steady, uniform EOF, as revealed by Eq. 20. In this case, induced internal pressures do not affect the results until $O((\gamma - 1)^2)$. It follows, therefore, that in the zeta potential measurement, the relative error caused by the conductivity mismatch is $O((\gamma - 1)^2)$. Because $|\gamma - 1| \ll 1$, Eq. 19, written back to the dimensional form, can be approximated as $I \approx I_2(1 - (\gamma - 1)(t/\tau))$ with $\tau = L/U$. As U is proportional to the zeta potential, the approximated form above provides a simple relationship between the zeta potential and the transient current. This furnishes the basis of the current monitoring method for measuring the surface zeta potentials of charged channels, as commonly employed in practice.

Note that Eqs. 19 and 20 are not limited to the case for small conductivity difference considered here. They are also applicable to the system whose conductivity difference is not small but zeta potential is high. As mentioned in Sect. 2, as long as the surface field is sufficiently high that $\ln(\lambda z e \mid E_s \mid /k_B\widetilde{T})$ is much larger than $|\ln(\gamma)|/2$, the zeta potentials in the two solutions will not differ significantly. In this case, setting $\beta = 1$, will give the identical result, despite the presence of the induced pressure flow. We also carry out direct numerical simulations using a commercial package (CFD-ACE+, version 2004) to confirm Eq. 19 under the constant zeta potential condition. Figure 2 shows that for various values of γ all the data can be collapsed into a single curve according to Eq. 19. The significance of this finding is that the use of Eq. 19 in the current monitoring method for measuring zeta potentials is not limited to systems with small conductivity differences. For those having high zeta potentials, as often encountered in microfluidic devices, the zeta potentials can still be accurately measured without having to worry about the effects of the induced pressure flow. In addition, it allows one to use solutions having a larger conductivity difference for rendering a greater change in the transient current.

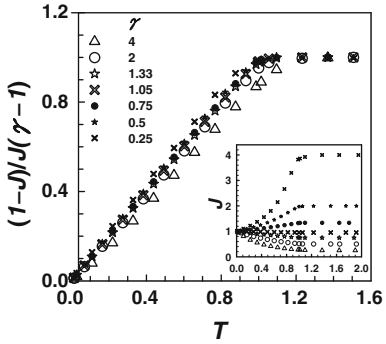

Fig. 2 Collapse of numerically simulated transient current data verse time for the constant surface zeta potential case. All the data with various conductivity ratios are collapsed into a universal curve according to $J = (1 + (\gamma - 1)T)^{-1}$. The *inset* displays the original data before collapsing them. The data for $\gamma = 4$ appears slightly deviated from the others. The reason is that in the simulations molecular diffusion always exists to smear the solution interface. Such smearing can be further enhanced by hydrodynamic dispersion caused by the induced pressure flow. The larger γ, the stronger the pressure flow and hence the dispersion

3.2 Case (ii): $\gamma \ll 1$

In this case, the fluid is displaced by a very high conductivity solution. To find the correct asymptotic behavior for J and X, it is not possible to simply take the $\gamma \to 0$ limit for Eqs. 17 and 18. Instead, it requires careful inspections on the original set of Eqs. 15 and 16. First of all, we inspect Eq. 15 after substitution of $\alpha = \gamma - 1$:

$$J = (1 + (\gamma - 1)X)^{-1}.$$

For $\gamma \ll 1$, the above equation indicates that the current increases as the interface moves and climbs rapidly when the interface approaches the exit of the channel, i.e., $J\,(X \to 1) \to \gamma^{-1}$. Neglecting γ, we find

$$J \approx (1 - X)^{-1}, \tag{21}$$

which will become unbounded as $X \to 1$. At first glance, such a singular behavior seems unphysical, but it is not. This is because decreasing γ here means increasing the conductivity of the displacing phase, while keeping the conductivity of the displaced phase fixed. At the end of the displacement, the channel is filled with the higher conductivity displacing phase. Therefore, an unlimited increase in its conductivity ($\gamma \to 0$) will raise the current indefinitely.

As for Eq. 16, it can be re-written in the approximated form below by incorporating $J \approx (1 - X)^{-1}$ in the $\gamma \to 0$ limit and keeping the terms up to $O(\gamma)$:

$$\frac{dX}{dT} = 1 + (\beta - 1)\gamma XJ \approx 1 - \frac{\gamma X}{1 - X}. \tag{22}$$

So, during most of the displacement, the interface's speed will be slightly lower than its initial value and decrease as

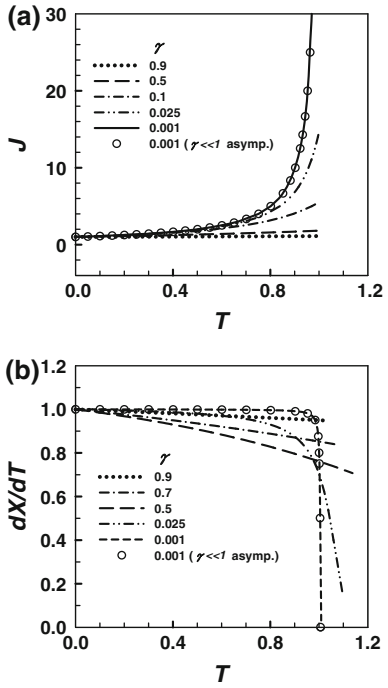

Fig. 3 Dependence of **a** the transient current J and **b** the displacement speed dX/dT on time T for displacement toward a lower conductivity solution ($\gamma < 1$) when $\beta = \gamma^{1/2}$. The asymptotic results (symbols) for $\gamma \ll 1$ are evaluated at $\gamma = 0.001$

the interface travels, except near the exit where the speed will decline very rapidly. Solving Eq. 22, we obtain the asymptotic solution for $X{:}X - \gamma \ln(1 - X) = T$. The corresponding current and interface speed can then be found by substituting the above into Eqs. 21 and 22.

In Fig. 3, we plot both electric current and displacement speed as functions of time for various values of $\gamma < 1$. At a sufficiently small γ, the asymptotic results are shown to be in excellent agreement with the exact ones calculated by Eqs. 17 and 18. Hence, the analysis here can indeed reveal the features for this limiting scenario. In Fig. 3b, the traveling speed for small γ seems to behave differently compared to others. This can be explained by considering three scenarios: $\gamma \approx 1$, non-small $\gamma < 1$, and $\gamma \ll 1$. For $\gamma \approx 1$, it is clear that the interface's speed remains constant U_2 throughout the displacement. As for non-small $\gamma < 1$, it corresponds to the displacement by a higher conductivity solution. In this case, because the channel will be progressively filled by the higher conductivity solution in which the slip velocity is slower, the interface's speed will gradually decrease as it moves. When $\gamma \ll 1$, however, the interface movement is dominated by the very fast slip velocity U_2 in the very low conductivity displaced phase. So its speed will be kept nearly as U_2, except near the exit where the speed declines very rapidly to U_1. Because the interface speed is constant for $\gamma \approx 1$, gradually decreases with position for non-small $\gamma < 1$, and then

turns nearly unchanged during the displacement (except near the exit) for $\gamma \ll 1$, these features imply that how the behavior of the interface speed varies with γ is not monotonic, which explains the crossovers between the transient current curves shown in Fig. 3b.

3.3 Case (iii): $\gamma \gg 1$

Here, we look at the scenario where a very low conductivity solution is used as the displacing phase. Since we restrict our attention to the thin double layer scenario with $\lambda_2/H \ll 1$ and $\lambda_1/H = (\lambda_2/H)\ \gamma^{1/2} \ll 1$, the constraint $\gamma \ll (\lambda_2/H)^{-2}$ must be imposed, where λ_1 and λ_2 are the respective double layer thicknesses for the displacing phase and the displaced phase. We again derive the asymptotic forms for Eqs. 15 and 16 at large γ:

$$J \approx (1 + \gamma X)^{-1}. \tag{23}$$

$$\frac{\mathrm{d}X}{\mathrm{d}T} \approx 1 + \gamma^n X J. \tag{24}$$

In Eqs. 23 and 24, although $\gamma \gg 1$, we retain "1"on the right-hand side in order to ensure $J = 1$ and $\mathrm{d}X/\mathrm{d}T = 1$ at $T = 0$ (because $X = 0$ in both Eqs. 15 and 16). Substituting Eq. 23 into Eq. 24, we can solve for X from Eq. 24, and hence J from Eq. 23. The results (with $n > 1$) are

$$\ln\left(1 + \gamma^{n-1}\left(J^{-1} - 1\right)\right) + \left(J^{-1} - 1\right) = \gamma^n T, \tag{25}$$

$$\ln(1 + \gamma^n X) + \gamma X = \gamma^n T. \tag{26}$$

How $\mathrm{d}X/\mathrm{d}T$ varies with T can then be determined by substituting Eqs. 25 and 26 into Eq. 24. Note that the logarithm terms in Eqs. 25 and 26 will not exist if one solves Eqs. 23 and 24 at leading order in γ (by dropping "1" on the right-hand side). To aid in understanding these asymptotic results, we inspect relevant scales below. First of all, since the total resistance is dominated by a very low conductivity displacing phase and varies as $\sim\gamma$, the current will drop like $J \sim \gamma^{-1}$ soon after the displacement starts, as revealed by Eq. 23. Since the fluid transport is also controlled by the displacing phase via $\mathrm{d}x_f/\mathrm{d}t \sim U_1 = v_1 E_1 \propto \sigma_1^{-n}\ I$ or $\mathrm{d}X/\mathrm{d}T \sim \gamma^n J$ from Eq. 24, this in conjunction with $J \sim \gamma^{-1}$ and $X \sim O(1)$ suggests that the displacement time will become very short: $T \sim \gamma^{-(n-1)}$, as also revealed by Eq. 26 (in the form without the logarithm term). With $T \sim \gamma^{-(n-1)}$, the scaling $J \sim \gamma^{-1}$ is also consistent with Eq. 25 (in the form without the logarithm term). Figure 4 displays how the transient current and displacement speed vary with time for various values of $\gamma > 1$. We also find that the asymptotic solution is in excellent agreement with the exact solution for a sufficiently large γ. It is clear that the larger γ, the closer the asymptotic solution will be compared to the exact solution, since the deviation of the former to the latter is $O(1/\gamma)$.

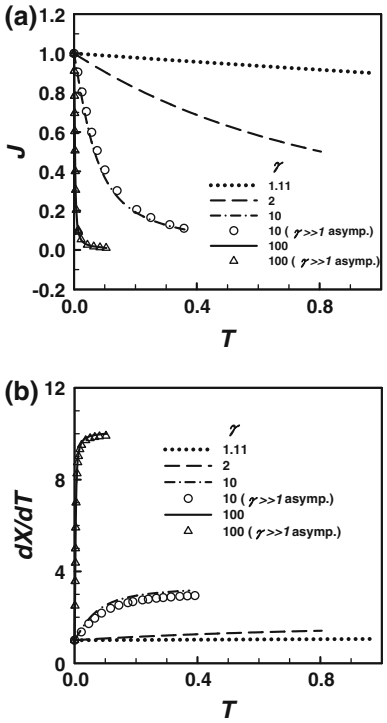

Fig. 4 Dependence of **a** the transient current J and **b** the displacement speed $\mathrm{d}X/\mathrm{d}T$ on time T for displacement toward a higher conductivity solution ($\gamma > 1$) when $\beta = \gamma^{1/2}$. *Circle* and *triangle symbols* are the $\gamma \gg 1$ asymptotes evaluated at $\gamma = 10$ and $\gamma = 100$, respectively

4 Extension to displacement involving multiple solution zones

Our analysis can also be extended to the situation involving more than two solutions. This can simply be realized by generalization of Eqs. 3 and 13 by taking the length average on the local electric fields (or the solution resistances), and the EOF slip velocities involved—the consequence of the electrics–hydrodynamics analogy. For a system containing N different solution zones, the electric current and the mean flow velocity can be shown to have the following forms:

$$I = V_0 \left(\sum_{i=1}^{N} f_i R_{iL} \right)^{-1}, \tag{27}$$

$$\bar{U} = \sum_{i=1}^{N} f_i U_i, \tag{28}$$

where $R_{iL} = \ell_i/\sigma_i$ is the resistance in zone i of length ℓ_i and conductivity σ_i, and $f_i = \ell_i/L$ is the corresponding length

fraction occupied in the channel. Let x_{ij} be the position of the interface between zone i and zone j. Then all the interfaces must move at the identical speed $\mathrm{d}x_{ij}/\mathrm{d}t = \bar{U}$ to satisfy fluid mass conservation. Using Eqs. 27 and 28, one can model electric flow and fluid transport for any displacement process containing an arbitrary number of solutions in series. To illustrate the features of such a process, we take a three-solution system as a case study below.

Initially, the system is filled with solution 3. Upon the displacement being set off by an electric field, solution 2 enters the channel first and then solution 1. From Eq. 27, the transient current is

$$J = \frac{1}{\gamma_{31}X_{12} + \gamma_{32}(X_{23} - X_{12}) + (1 - X_{23})}, \tag{29}$$

where $J = I/I_3$ is the current scaled by $I_3 = \sigma_3 V_0/L$, $\gamma_{31} = \sigma_3/\sigma_1$ and $\gamma_{32} = \sigma_3/\sigma_2$ are the conductivity ratios, and $X_{12} = x_{12}/L$ and $X_{23} = x_{23}/L$ are the displacement distances of the two solution interfaces normalized by the channel length. The corresponding fluid transport equation is

$$\frac{\mathrm{d}X_{ij}}{\mathrm{d}T} = (\gamma_{31}\beta_1 X_{12} + \gamma_{32}\beta_2(X_{23} - X_{12}) + (1 - X_{23}))J, \tag{30}$$

where X_{ij} can be either X_{12} or X_{23}, $\beta_i = v_i/v_3$ ($i = 1, 2$) the mobility ratios, and $T = t/\tau$ with $\tau = L/(v_3 E_0)$.

Equations 29 and 30 can be used to describe a process involving successive displacements in which there are no more than three solutions staying within the channel. When the process involves only two solutions, the above equations with $X_{12} = 0$ or $X_{12} = X_{23}$ reduce to Eqs. 15 and 16 for two-solution systems. If all the three solutions stay in the channel, since the interfaces are traveling at the same speed, the length of the middle solution zone will be invariant with time (i.e., $X_{23} - X_{12} =$ constant) until its leading edge exits the channel. In this case, the middle zone acts like a plug, contributing an additional resistance to the electric flow, but increasing the mobility of the fluid flow according to Eqs. 29 and 30: $J = (\gamma_{31}X_{12} + R' + (1 - X_{23}))^{-1}$ and $\mathrm{d}X_{ij}/\mathrm{d}T = (\gamma_{31}\beta_1 X_{12} + \beta_2 R' + (1 - X_{23}))J$ with $R' = \gamma_{32}(X_{23} - X_{12})$ = constant. For given lengths of the solutions, Fig. 5 shows transient current responses for a variety of solution arrangements. It reveals that transient currents in these systems can undergo non-monotonic and stagewise changes, depending on the conductivity ratios of these solutions.

5 Effects of surface conductance

For a highly charged surface immersed in an electrolyte solution (especially containing multivalent ions), more counterions will be condensed onto the surface, forming a compact charge layer much thinner than the diffuse Debye layer. These condensed counterions increase the conductivity of the double layer, making it more conducting than the bulk if the surface charge is sufficiently high. As this condensed charge layer acts like a thin conducting sheet overlaying the surface, it contributes an extra surface current to the electric flow, creating the so-called surface conductance effect that can increase the apparent conductivity of a solution (Dukhin and Derjaguin 1974). In other words, the situation looks like two resistors in parallel: one is the lower conductivity bulk resistor having a large cross-sectional area, and the other is the higher conductivity surface layer of a much narrower current passage.

As a result, the total current due to enhancement by surface conductance K_s reads

$$I = \sigma EA + K_s ES = \sigma(1 + K_s S/\sigma A)EA. \tag{31}$$

Here σEA is the Ohmic current passing through the cross sectional area A and $K_s ES$ is the excess surface current around the perimeter S of the channel. Combining these two contributions gives the effective conductivity $\sigma(1 + K_s S/\sigma \mathrm{A})$. For a two-dimensional channel whose width W is much larger than the channel height H, the area-to-perimeter ratio $A/S \approx H/2$. In this case, the effective conductivity can be approximated as

$$\sigma_{\mathrm{eff}} = \sigma\left(1 + \frac{K_s}{\sigma A/S}\right) \approx \sigma\left(1 + \frac{2K_s}{\sigma H}\right) = \sigma(1 + 2Du). \tag{32}$$

Here the Dukhin number, $Du = K_s/\sigma H$, measures the magnitude of the conductivity enhancement relative to the bulk conductivity. As contributions to the system's conductivity actually involve the Stern layer conductivity (due to bound charges), the diffuse layer conductivity, and the bulk conductivity, how the system's conductivity is determined by these conductivities would depend on the surface zeta potential, the thickness of the diffuse layer, and the size of the Stern layer, as can be revealed by analyzing the behavior of the streaming potential in a charged channel (Das and Chakraborty 2010). Effects at the atomic level, such as ion correlation (Kjellander 2009) and steric effects (Borukhov and Andelman 1997), could also come into play to modify the structure of the double layer, depending on interactions between compacted charges and the size of these charges. Nevertheless, as it is the collapsed charge layer within the diffuse Debye layer contributing to most of the surface conductance, in what follows we exclude the contributions from the Stern layer and ion size effects to see how this layer impacts the displacement in a highly charged channel.

We start with the following relationship that links the Dukhin number to the zeta potential (Lyklema 1995):

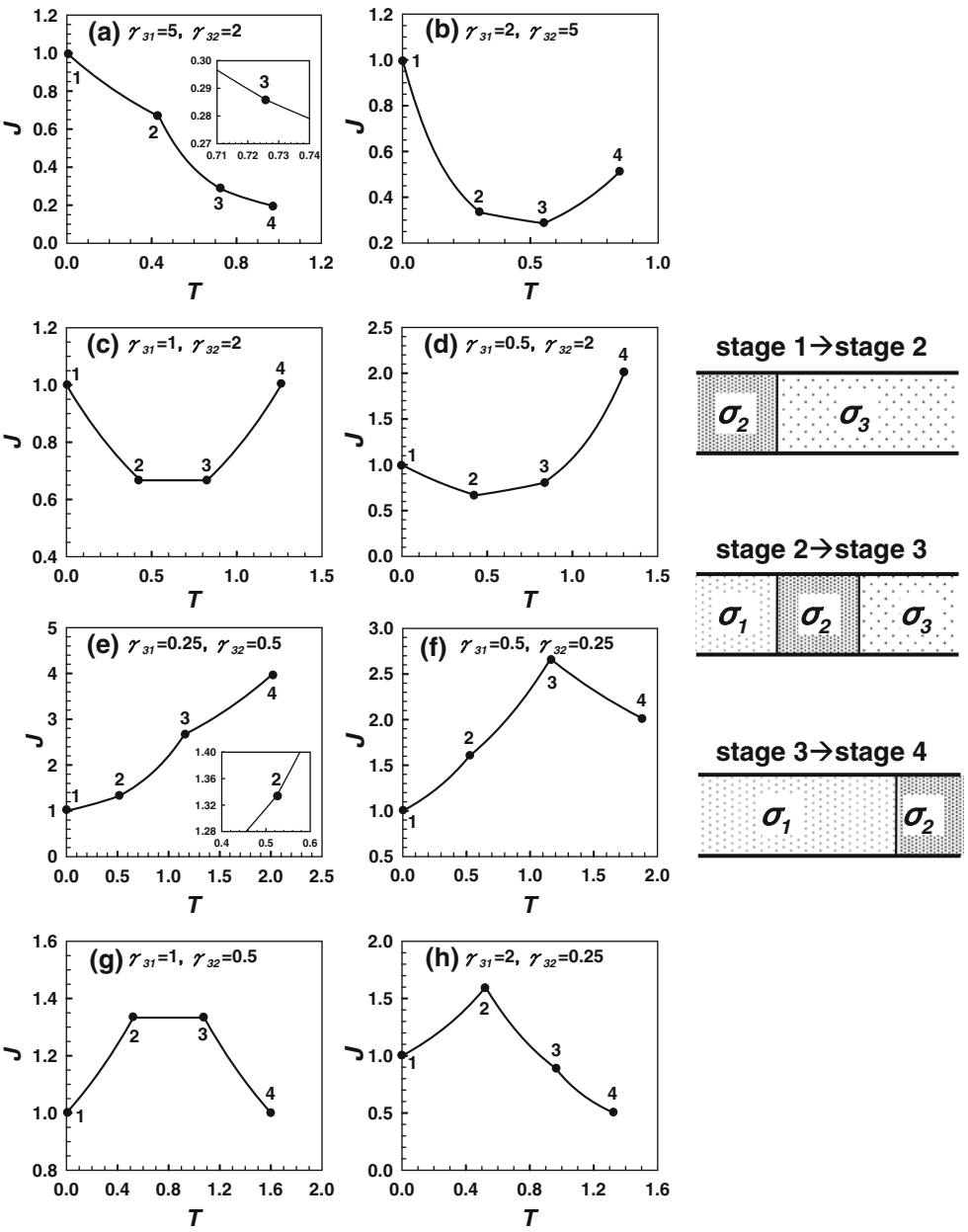

Fig. 5 Stagewise transient current responses in successive displacements involving three solution zones at $X_{23} - X_{12} = 0.5$ and $\beta = \gamma^{1/2}$. The figures on the right are to illustrate different stages during a displacement. Various behaviors are observed, depending on the conductivity ratios $\gamma_{31} = \sigma_3/\sigma_1$ and $\gamma_{32} = \sigma_3/\sigma_2$ between the solutions. **a** $\gamma_{31} > \gamma_{32} > 1$, **b** $\gamma_{32} > \gamma_{31} > 1$, **c** $\gamma_{32} > 1$ and $\gamma_{31} = 1$, **d** $\gamma_{32} > 1 > \gamma_{31}$, **e** $1 > \gamma_{32} > \gamma_{31}$; **f** $1 > \gamma_{31} > \gamma_{32}$; **g** $\gamma_{32} < 1$ and $\gamma_{31} = 1$, and **h** $\gamma_{31} > 1 > \gamma_{32}$. In **e**, the value of J at the end of the displacement looks greater than those in the others. It is because we choose $\gamma_{31} = \sigma_3/\sigma_1 = 0.25$ here, the current at the end of the displacement must be four times that at the beginning of the displacement

$$Du = \frac{K_s}{\sigma H} = \frac{2\lambda}{H}\left[\cosh\left(\frac{ze\zeta}{2k_B\widehat{T}}\right) - 1\right], \tag{33}$$

where $\lambda = \left(\varepsilon k_B\widehat{T}/2z^2e^2C_\infty\right)^{1/2} = (D\varepsilon/\sigma)^{1/2}$ is the thickness of the Debye layer, with C_∞ being the electrolyte concentration, σ the conductivity, z the valence of the electrolyte (which is assumed symmetric), and D the ionic diffusivity. How the zeta potential depends on the Debye layer thickness λ and the surface charge density q_s of the surface can be determined by the Gouy–Chapman theory (Lyklema 1995):

$$\sinh\left(\frac{ze\zeta}{2k_B\widehat{T}}\right) = \mathrm{sign}(q_s)\frac{\lambda}{2\delta}, \tag{34}$$

where $\delta = \varepsilon k_B\widehat{T}/ze|q_s|$ is the Gouy–Chapman length measuring the thickness of the collapsed layer—the higher ζ, the thinner δ (provided that the surface charge density q_s is constant since a charged surface is usually covered by a *fixed* number of ionizable groups). With the aid of Eq. 34, the Dukhin number defined by Eq. 33 can be re-expressed in terms of ratios between relevant length scales:

$$Du = \frac{K_s}{\sigma H} = \frac{2\lambda}{H}\left[\left(\left(\frac{\lambda}{2\delta}\right)^2 + 1\right)^{1/2} - 1\right] \approx \left(\frac{\lambda}{\delta}\right)^2 \left(\frac{\delta}{H}\right), \tag{35}$$

wherein λ/δ is generally large. As a result, the effective conductivity increases as the channel height is decreased, since the conducting collapsed layer sheet becomes relatively thicker. Equation 35 also indicates that surface conductance can be negligible if $Du \ll 1$ for low ζ (large δ) or small λ/H. If the channel is small and highly charged such that $Du \geq 1$, σ_{eff} could become significantly larger than the native value σ. For instance, consider a channel with $\lambda/H = 0.1$ and $\zeta \sim 100$ mV in a divalent electrolyte solution ($z = 2$). λ/δ is about 55 estimated from Eq. 34, and hence $Du \approx 5.5$ from Eq. 35, giving rise to a significant increase in the effective conductivity: $\sigma_{\text{eff}} \approx 12\sigma$, as given by Eq. 32.

We now examine how surface conductance influences the features of the displacement. As the effective conductivity can increase with surface conductance in either solution, we inspect the actual conductivity ratio to see if the behavior of the transient current can undergo qualitative changes due to surface conductance effects. By replacing the native conductivities with the effective ones and making use of Eq. 32, the actual conductivity ratio $\gamma_{\text{actual}} = \sigma_{\text{eff }2}/\sigma_{\text{eff }1}$ reads

$$\gamma_{\text{actual}} = \gamma\frac{1 + 2Du_2}{1 + 2Du_1} = \gamma\frac{1 + 2(\lambda_2/\delta)^2(\delta/H)}{1 + 2\gamma(\lambda_2/\delta)^2(\delta/H)}, \tag{36}$$

in which $Du_1 = \gamma\, Du_2$ because of $\lambda_1 = \lambda_2\gamma^{1/2}$. Obviously, for $H \to \infty$, $\gamma_{\text{actual}} \to \gamma$, as it must be. In the $H \to 0$ limit, we find $\gamma_{\text{actual}} \to 1$. We also observe that for $\gamma > 1$, $\gamma_{\text{actual}}/\gamma < 1$ and decreases as H is decreased, whereas for $\gamma < 1$, $\gamma_{\text{actual}}/\gamma > 1$ and increases when reducing H. But in either case ($\gamma_{\text{actual}} - 1$) will never change the sign, as can be seen from Eq. 36 in the alternative form: $\gamma_{\text{actual}} = 1 + (\gamma - 1)/(1 + 2\gamma(\lambda_2/\delta)^2(\delta/H))$. As such, although the effective conductivities of both the solutions can be increased by surface conductance effects, this does not change their numerical order. Hence, the behavior of the transient current will not alter qualitatively.

The conclusion drawn above is based on the use of the same electrolyte. No qualitative change in the behavior of transient current in such a case can be attributed to the fact that the effective conductivities of the two solutions increase with surface conductance at an equal rate, making ($\gamma_{\text{actual}} - 1$) never change the sign. Therefore, to render the sign change of ($\gamma_{\text{actual}} - 1$) so as to change the trend of transient current, one might require unequal increments in the effective solution conductivities, which can only be realized when the solutions have different valences (provided that the surface charge density is fixed). To see this, we notice in Eq. 35, together with the Gouy–Chapman length $\delta = \varepsilon k_B\hat{T}/ze|q_s|$, that for given surface charge density and solution conductivity, Du is proportional to the solution's valence z. So, the rise of the effective conductivity of a polyvalent solution by surface conductance can become more apparent than that of a monovalent solution at the same ionic strength. As this effect can be enhanced by decreasing the bulk conductivity and by lowering the channel height, one can imagine that if the lower conductivity solution has a greater valence than the higher conductivity solution, the effective conductivity of the former could rise more quickly than the latter as the channel height is decreased. At the point where the effective conductivity of the lower conductivity solution exceeds that of the higher one, the transient current will be turned over and become opposite to those usually seen in large channels.

To see how such a turnover event occurs and to illuminate how the electrolyte valences modify the actual conductivity ratio, we let $\chi \equiv \delta_2/\delta_1 = z_1/z_2$, and rewrite Eq. 36 by substituting $Du_1 = \gamma\chi Du_2$:

$$\gamma_{\text{actual}} = \gamma\frac{1 + 2Du_2}{1 + 2\gamma\chi Du_2} = \gamma\frac{1 + 2(\lambda_2/\delta_2)^2(\delta_2/H)}{1 + 2\gamma\chi(\lambda_2/\delta_2)^2(\delta_2/H)}. \tag{37}$$

Because $\gamma_{\text{actual}}\ (H \to \infty) \to \gamma$ but $\gamma_{\text{actual}}\ (H \to 0) \to \chi^{-1}$, we find that for $\gamma > 1$ and $\chi > 1$, $\gamma_{\text{actual}} > 1$ can turn to be <1 at a sufficiently small H. Similarly, for $\gamma < 1$ and $\chi < 1$, $\gamma_{\text{actual}} < 1$ can switch to >1 when H is decreased to a certain value. That is, ($\gamma_{\text{actual}} - 1$) can now change the sign, making the transient current behavior turned the opposite to that in a large channel. At the critical state where $\gamma_{\text{actual}} = 1$, the transient current remains constant throughout displacement. So there must exist the critical channel height H^* (or the critical Dukhin number Du_2^*) below (beyond) which the transient current can be flipped by surface conductance effects.

Solving Eq. 37 at $\gamma_{\text{actual}} = 1$, we find

$$H^* \approx 2\delta_2\left(\frac{\lambda_2}{\delta_2}\right)^2\gamma\left(\frac{\chi - 1}{\gamma - 1}\right) \quad \text{or} \quad Du_2^* \approx \frac{1}{2\gamma}\left(\frac{\gamma - 1}{\chi - 1}\right). \tag{38}$$

Equation 38 indicates that at $\chi = 1$, $H^* \to 0$ or $Du_2^* \to \infty$, recovering the result that it is unattainable to flip the transient current in the equal-valence case. Equation 38 further reveals that for $\gamma > 1$ (<1), H^* or Du_2^* can exist only if $\chi > 1$ (<1). Moreover, because $Du_1 = Du_2\gamma\chi$, the sign inversion of ($\gamma_{\text{actual}} - 1$) takes place either when $Du_1 > Du_2 > Du_2^*$ for $\gamma > 1$, or when $Du_2 > Du_2^* > Du_1$ for $\gamma < 1$. That is, flipping transient current is only possible if the surface conductance of the lower conductivity solution is greater than that of the

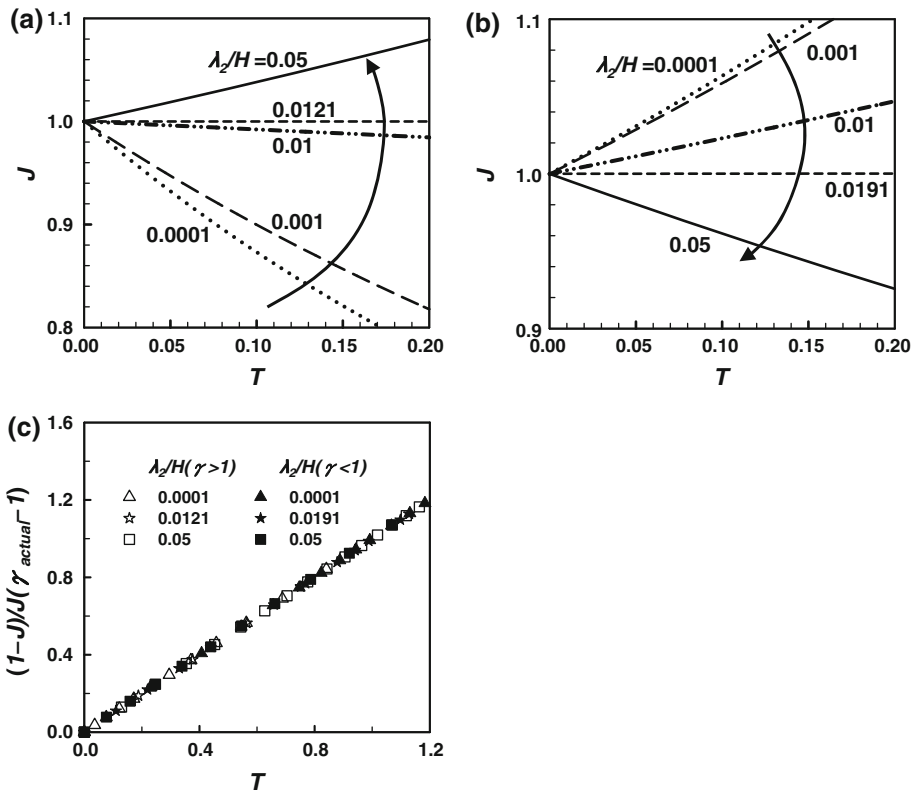

Fig. 6 Flipping of transient current due to surface conductance effects in highly charged channels with $\beta = \gamma^0$ when the ratio of the Debye layer to the channel depth, λ_2/H, is greater than some critical value. **a** $\gamma = 2.5$, $\chi = 2$, and **b** $\gamma = 0.4$, $\chi = 0.5$. In **a** and **b**, the critical values of λ_2/H are 0.0121 and 0.0191, respectively. In **c**, all the data with various values of λ_2/H in **a** and **b** are collapsed into a universal curve according to $J = (1 + (\gamma_{\text{actual}} - 1)T)^{-1}$

higher conductivity one to cause the effective conductivity of the former to exceed that of the latter.

Replacing γ by γ_{actual} given in Eq. 37, we apply the exact solution Eq. 18 in Sect. 3 to re-calculate the transient currents in displacements using electrolyte solutions having unequal valences. Figures 6a and b reveal that the transient current can indeed be flipped over due to the exceeding conductivity enhancement in the lower conductivity solution mentioned above. Similar to Fig. 2 for channels with high zeta potentials, all the transient current curves in Figs. 6a and b can be collapsed into a universal curve according to $J = (1 + (\gamma_{\text{actual}} - 1)T)^{-1}$, as shown in Fig. 6c.

6 Effects of diffusion smearing and hydrodynamic dispersion

In an actual displacement, because of the solution conductivity mismatch, diffusion always exists at the place where the two solutions meet. Therefore, the solution interface will be inevitably smeared by diffusion, creating a mixing zone of length $\ell \sim (Dt)^{1/2}$ between the solutions. In addition, hydrodynamic dispersion (Taylor 1953) arising from the induced pressure flow could further broaden the zone. In this section, we briefly discuss how these effects mediate the displacement.

We first consider effects of diffusion smearing. Assume that diffusion is sufficiently fast so that any electrolyte concentration variations across the streams are smeared out. This assumption is valid if the diffusion time across the channel depth is sufficiently short compared to the displacement time, i.e., $H^2/D \ll L/U$ or $Pe_L \ll (L/H)^2$. Having assumed fast transverse diffusion, we can then simplify the problem and adopt the length-averaged formalism to determine the electric resistance and the displacement speed by including the contribution from the mixing zone:

$$R = \frac{x_f - \ell/2}{\sigma_1} + \int_{-\ell/2}^{\ell/2} \frac{\mathrm{d}x'}{\sigma_d} + \frac{L - x_f - \ell/2}{\sigma_2}, \tag{39}$$

$$\frac{\mathrm{d}x_f}{\mathrm{d}t} \equiv \bar{U} = \left(\frac{x_f - \ell/2}{L}\right) U_1 + \frac{1}{L} \int_{-\ell/2}^{\ell/2} U_d \mathrm{d}x' + \left(\frac{L - x_f - \ell/2}{L}\right) U_2, \tag{40}$$

where σ_d is the conductivity and U_d is the slip velocity in the zone. The integral terms in Eqs. 39 and 40 represent the averaged resistance and velocity over the mixing zone, respectively. These integrals are carried out in the frame moving with the front $x' = x - x_f$, with the actual front

position x_f (and hence the displacement speed) being defined at the position where the pressure gradient vanishes. Making use of the fact that the EOF velocity varies with conductivity according to $U_i \propto \sigma_i^{-n}$ $(n > 0)$ (see Sect. 2), we write $U_1 = U_2\,(\sigma_2/\sigma_1)^n$ and $U_d = U_2\,(\sigma_2/\sigma_d)^n$ in Eqs. 39 and 40 to recast these equations as

$$R = \frac{L}{\sigma_2}\left[1 + (\gamma - 1)\left(\frac{x_f}{L}\right) + \frac{\ell}{L}\left(\int_{-1/2}^{1/2}\left(\frac{\sigma_2}{\sigma_d}\right)\mathrm{d}z - \frac{\gamma + 1}{2}\right)\right], \tag{41}$$

$$\bar{U} = U_2\left[1 + (\gamma^n - 1)\left(\frac{x_f}{L}\right) + \frac{\ell}{L}\left(\int_{-1/2}^{1/2}\left(\frac{\sigma_2}{\sigma_d}\right)^n\mathrm{d}z - \frac{\gamma^n + 1}{2}\right)\right], \tag{42}$$

with $z = x'/\ell$. As a result, the corrections to the resistance and the displacement speed, reflected by the respective ℓ/L terms in Eqs. 41 and 42, turn out to be the corresponding deviations of the length-averaged quantities in the mixing zone to the mean values of the two bulk solutions. In the special case of $n = 1$ where the EOF mobility is independent of solution conductivity in the high zeta potential regime, we find that the terms in the parentheses in Eqs. 41 and 42 are identical, i.e., $R/(L/\sigma_2) = \bar{U}/U_2$. In this case, since $U_2 = v_2E_2 = v_2I/\sigma_2 = (v_2/\sigma_2)(V_0/R)$, the displacement speed $\bar{U} = v_2V_0/L = v_2E_0$ is constant throughout the displacement despite the presence of diffusion smearing. Therefore, diffusion smearing can only affect the transient current through variations of the resistance.

As such, if the conductivity distribution in the mixing zone can be found, we can in principle quantify effects of diffusion on the transient current and the displacement speed using Eqs. 41 and 42. Here, we do not intend to carry out a complete analysis for the electrolyte transport in the zone. Instead, we illuminate the effects analytically by considering a nearly uniform displacement situation with $|\gamma - 1| \ll 1$ (see Sect. 3.1). Since the diffusion boundary layer will develop from the moving front to penetrate into the two solutions with thickness growing like $(Dt)^{1/2}$, the electrolyte transport in the zone, if looking at the system in the frame moving with the front, will be simply governed by diffusion equation—a constant velocity will not produce any transport. The situation here is similar to the startup problem due to pure diffusion, but takes place at the constant moving front. Therefore, the conductivity distribution in the zone $\sigma_d\,(x')$ must bear a self-similar form described by the combined variable $\xi = x'/(\ell(t)/2)$ with $x' = x - \bar{U}t$:

$$\frac{\sigma_d - \bar{\sigma}}{\sigma_2 - \bar{\sigma}} = \mathrm{erf}\left(\frac{x'}{\ell(t)/2}\right), \tag{43}$$

which satisfies $\sigma_d\ (x' \to \infty) = \sigma_2$ and $\sigma_d\ (x' \to -\infty) = \sigma_1$. Here $\bar{\sigma} = (\sigma_1 + \sigma_2)/2$ is the mean conductivity of the two solutions and erf is the error function. Because the zone can be expanded (compressed) by the outward (inward) pressure flow for $\gamma > 1$ $(\gamma < 1)$ (in the frame moving with the front), we expect that the actual width of the zone $\ell(t)$ should behave like $2(Dt)^{1/2}\,(1 + f)$ in which $f > 0$ (< 0) reflects the correction due to the conductivity mismatch when $\gamma > 1$ (< 1).

We can then apply Eq. 43 to find the electric resistance of the zone. For $|\gamma - 1| \ll 1$ the result can be approximated as

$$R_d = \int_{-\ell/2}^{\ell/2}\frac{\mathrm{d}x'}{\sigma_d} \approx \frac{\ell}{\bar{\sigma}}\int_{-1/2}^{1/2}\left(1 - \left(\frac{\sigma_2}{\bar{\sigma}} - 1\right)\mathrm{erf}(z)\right)\mathrm{d}z \approx \frac{\ell}{\bar{\sigma}}, \tag{44}$$

in which the integral involving the error function is identically zero. It turns out that the apparent conductivity of the zone is simply the mean of the two bulk values, which is not surprised. So the correction to the resistance due to diffusion smearing can be found from the ℓ/L term in Eq. 41, giving

$$\begin{aligned}\Delta R \equiv R_d - \frac{\ell}{2\sigma_2}(\gamma + 1) &\approx -\frac{\ell}{2\sigma_2}(\gamma - 1)^2(1 + \gamma)^{-1} \\ &\approx -\frac{\ell}{4\sigma_2}(\gamma - 1)^2,\end{aligned} \tag{45}$$

which occurs at $O((\gamma - 1)^2)$. As the resistance now is slightly reduced by diffusion smearing, the electric current with diffusion will be slightly higher than that without.

In the above discussion, we consider the effects arising solely from molecular diffusion. We now take into account hydrodynamic dispersion that can promote diffusion smearing due to the enhancement of the axial diffusion coefficient by the induced pressure flow. How hydrodynamic dispersion impacts the extent of the mixing zone can be pictured as follows. Because of the transverse velocity gradient setup by viscous shearing, electrolyte molecules, especially along the edge of the mixing zone, at different transverse positions are advected at different speeds, creating a concentration gradient across the streams and hence resulting in additional diffusion in the transverse direction. Together with the pre-existed concentration gradient in the streamwise direction, the mixing zone can then be broadened at a much faster rate than that by molecular diffusion alone. The phenomenon is in effect equivalent to the spreading of electrolytes with an enhanced diffusion coefficient. In our system, the effective diffusion coefficient D_{eff} can be determined by modifying the classical result (Aris 1956):

$$\frac{D_{\text{eff}}}{D} = 1 + \Lambda\left(\frac{\Delta U H}{D}\right)^2, \tag{46}$$

where Λ is the geometrical factor and $\Delta U \equiv |U_2 - U_1|$ is the difference between the two slip velocities, as it is this velocity difference setting up the induced pressure flow responsible for the dispersion. Because $U_1/U_2 = \gamma^n$ $(n > 0)$, the relative slip velocity difference is $\Delta U/U_2 = \gamma^n - 1$ (in reference to the displaced phase with which the displacement starts), and hence we expect that the dispersion will become more pronounced for $\gamma > 1$.

7 Applicability of the analysis and comparison with experiments

Our analysis is based on the assumption that the interface always maintains flat and sharp during a displacement. This assumption holds only if the following two criteria are satisfied, as already discussed in Sect. 2.

First, the axial Peclet number $Pe_L = UL/D$ must be sufficiently large so that diffusion can be neglected compared to convection. With $U \sim 10^2$ μm/s, $L \sim 1$ cm, and $D \sim 10^{-5}$ cm^2/s in typical microfluidic experiments, the estimated Peclet number is $Pe_L \sim 10^3$. As the interface's broadening is merely 3% of the channel length, diffusion smearing is indeed unimportant in practice.

Second, to ensure that the flow is unidirectional in most of the channel, the width of the transition zone near the interface $Re \cdot H$ must be sufficiently small compared to the channel length L. Given $Re = 0.01$–0.1 and $H \sim 100$ μm in typical microfluidic experiments, the transition zone is no more than 10 μm and hence less than 0.1% of $L = 1$–10 cm. Therefore, possible interface distortion by the non-parallel flow in the zone can be safely neglected.

Combining $Pe_L \gg 1$ and $ReH \ll L$, we can find the range of the velocity scale for ensuring the applicability of the present analysis:

$$D/L \ll U \ll \nu L/H^2. \tag{47}$$

Using typical values $\nu \sim 10^{-2}$ cm^2/s, $D \sim 10^{-5}$ cm^2/s, $H \sim 100$ μm, and $L \sim 1$ cm, we find 10^{-5} cm/s $\ll U \ll 10^2$ cm/s. In most of the EOF experiments, velocity scales are within the range estimated above, justifying the applicability of the present analysis.

To see if our analysis can describe real EOF-driven displacement processes, we also compare our results with the existing experimental data. We first look at the work of Huang et al. (1988) who invented the current monitoring method for measuring the surface zeta potential of a capillary. In their work, by performing a nearly uniform displacement using solutions with a small conductivity mismatch, they tracked the transient current and found that it virtually varies linearly with time. In our analysis, we show analytically for $\gamma \approx 1$ case (see Sect. 3.1) that the transient current does reveal such a linear response. As seen in Fig. 7, our results match perfectly with their data for both $\gamma < 1$ and $\gamma > 1$ cases. In addition, we identify that relative errors in the measured zeta potentials due to the solution conductivity mismatch are $O((\gamma - 1)^2)$. In other words, our analysis not only is able to capture Huang et al.'s data but also justifies the use of the current monitoring method in measuring surface zeta potentials.

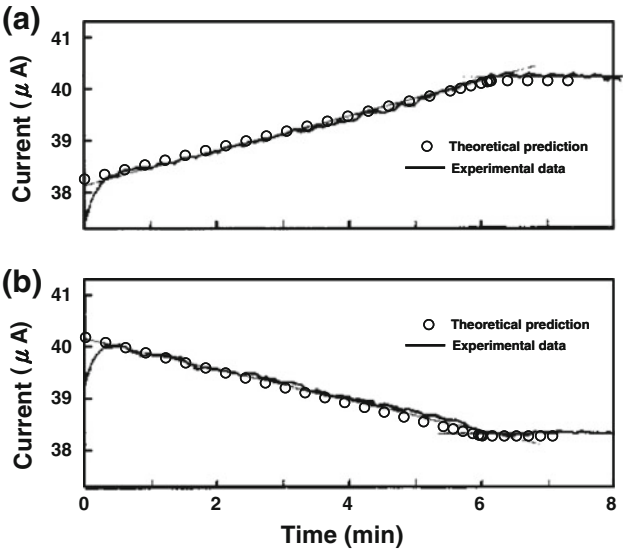

Fig. 7 Comparison between our theoretical predictions and the transient current data measured by Huang et al. (1988). Their experiments are conducted in a 63 cm-long capillary tube having inner diameter of 75 μm. The electric field is 33.3 kV/m. **a** Is the result with 20 mM phosphate buffer displacing 19 mM phosphate buffer ($\gamma = 0.95 < 1$). **b** Is obtained by flowing 19 mM phosphate buffer toward 20 mM phosphate buffer ($\gamma = 1.05 > 1$). The conductivities of 20 and 19 mM phosphate buffers are 2.73 and 2.6 mS/cm, respectively

Further experimental evidence for supporting our analysis can be seen in the work of Ren et al. (2003). In their experiments, the solution conductivity contrast was large, which can be considered as $\gamma \ll 1$ or $\gamma \gg 1$. They found that electric currents can show a quick rise near the end of a displacement for $\gamma \ll 1$ and decline very rapidly at the beginning of a displacement for $\gamma \gg 1$, as predicted, respectively, in Sects. 3.2 and 3.3. More quantitative comparison is also made in Fig. 8, showing that our theoretical predictions do agree well with their data. As these experimental results can be well predicted by our simplified equations, the present analysis does capture the essential physics of EOF-driven displacement.

8 Concluding remarks

We have analyzed EOF-driven displacement between two solutions in a uniformly charged microchannel and

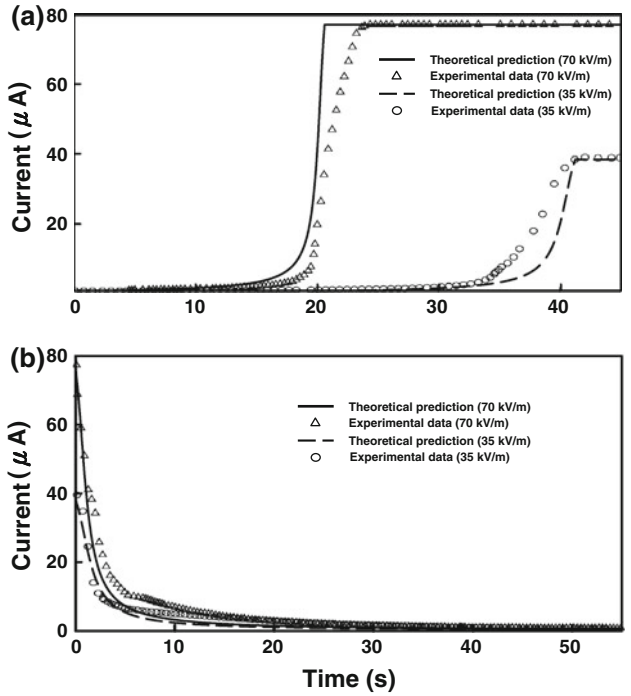

Fig. 8 Comparison between our theoretical predictions (*lines*) and the transient current data (*symbols*) measured by Ren et al. (2003). **a** Is obtained by flowing 10 mM KCl solution toward 0.1 mM KCl solution ($\gamma = 0.0107 \ll 1$), and **b** is the result with 0.1 mM KCl solution displacing 10 mM KCl solution ($\gamma = 93.3 \gg 1$). Experiments are carried out under electric fields 35 and 70 kV/m

examined how solution conductivity difference plays roles in the current monitoring method. A conductivity mismatch causes unequal EOF slip velocities in the solutions, producing internal pressures to affect the propagation of the solution interface and the behavior of the transient current. Despite these induced internal pressures, we verify that the interface can remain flat across the channel depth and be advected by the local plug flow. Analyzing both electric and fluid flow problems, we derive a coupled set of length-averaged equations to elicit how the electric current and the traveling distance of the solution interface vary with time, electric field, and the solution conductivities. We also show that the equation governing the interface's propagation can be readily obtained through the analogy to that derived from Ohm's law using the electrics-hydrodynamics similitude.

Effects of solution conductivity difference are illuminated by three different systems. For solutions with a small conductivity difference, we obtain the constant-speed displacement in a uniform EOF, recovering the result that the transient current changes linearly with time. In a displacement by a very high conductivity solution, the electric current rises very rapidly as the interface moves towards the exit of the channel. The displacement speed is found to only decrease slightly with time, except near the exit where it drops very rapidly. On the other hand, if the fluid is pushed by a very low conductivity solution, it will be advected at a very fast speed but with a dramatic decline in the electric current. In the high zeta potential regime, if the surface charge density were sufficiently high to outweigh the influence from the conductivity difference, the surface zeta potentials in the two solutions would not differ significantly. In this case, the result is essentially identical to that in the constant-speed displacement case, regardless of the conductivity ratio (as long as it is an order of unity). The present framework can also be applied to successive displacements involving multiple solution zones. In these systems, transient currents can vary with time in a non-monotonic and stagewise fashion, depending on the conductivities of the zones.

We also unravel the critical roles of surface conductance in highly charged channels by inspecting how transient currents are influenced by an additional conductivity arising from the existence of the collapsed counterion layer. The most important finding is that if the lower conductivity solution has a greater valence than the higher one, the apparent conductivity of the former can exceed that of the latter when the channel height is below some critical value. The effect turns the transient current behavior to be opposite to that in the usual large channel case. As this current flipping phenomenon is unique to displacements in highly charged submicron channels, it offers a new paradigm to gauge the importance of surface conductance. It is worth pointing out that such a current flipping phenomenon has not been observed in usual experiments, which can be explained by the following reasons.

First of all, the phenomenon can only be realized when solutions of different valences are used. In addition, in order to have appreciable surface conductance effects, the channel height cannot be too large compared to the Debye layer thickness. It cannot be too small, either; otherwise the double layers will become overlapped, to which the present analysis is clearly not applicable. Because of these constraints, we envisage that the phenomenon might occur in certain windows of the parameters and it is more likely to take place in a displacement involving two different polyvalent electrolyte solutions in a highly charged *submicron* channel. Therefore, whether the phenomenon can be observed would require a careful design of the channel dimensions in line with a judicious choice of solution conditions, which explains why the phenomenon has yet been observed in usual experiments. In future work, we will carry out experiments to see if the phenomenon can occur as predicted.

We also make attempts to elicit how diffusion smearing impacts the displacement by including the additional mixing zone into the analysis. When the solution conductivity difference is small, we find that the transient current

with diffusion is slightly greater than that without. If the solution conductivity difference is large, however, hydrodynamic dispersion could cause the mixing zone to be broadened at a much faster rate than that by molecular diffusion alone.

Our study provides renewed insights into the current monitoring method for measuring the surface zeta potentials of microchannels. In this method, one usually employs electrolyte solutions with a small conductivity difference to generate a nearly uniform sweeping for rendering a steady change of the transient current. As we have identified how transient current behaves for an arbitrary conductivity ratio, it is not necessary to use a small conductivity difference in the measurement; one can use solutions having a greater conductivity difference to render more sizeable changes in transient currents and still obtain the zeta potential in accuracy. Therefore, having the knowledge on how solution conductivity difference impacts the displacement, the applicability of the current monitoring method for characterizing surfaces of microchannels can be greatly extended. In fact, we have made comparison between our theoretical results and the existing experimental data of various solution conductivity ratios. We find that our results agree very well with the measured data. So our analysis does capture the natures of the displacement.

While this study is focused on solution displacement in which the electric double layers are much thinner than the channel height, it might be interesting to envisage what happens if displacing solutions in a nanochannel. As the double layers are now comparable to the channel height, the overlapping of the double layers no longer screens the surface charge of the channel. Consequently, the solution in the channel is not electro-neutral and driven entirely by the electric body force imparted by the net charge density multiplied by an applied electric field. The resulting EOF velocity obviously will depend on how ions are distributed within the channel. Moreover, if the channel height were below the double layer thickness, the bulk conductance would become independent of the electrolyte concentration, as opposed to the usual linear relationship (Stein et al. 2004; Yossifon et al. 2009). In this case, there could be no current change during the displacement. In addition, near the entrance and exit of the channel where the channel depth changes abruptly from nanometer to micrometer scales, or vice versa, the bulk conductance could undergo a dramatic change due to its different dependences on the electrolyte concentration. Moreover, concentration polarization could likely occur due to ion depletion/enrichment effects caused by the double-layer overlapping (Pu et al. 2004). Because these effects are either absent or negligible in our system, we expect that the features of displacing solutions in nanochannels would be quite different from those found in this work.

Acknowledgements This work was supported by the National Science of Council of Taiwan under Grants NSC 97-2628-E-006-001-MY3 of HHW and NSC 98-2221-E-006-098-MY3 of CHC. The authors would also like to thank the National Center for High Performance Computing in Taiwan for the use of computation facilities in generating part of the results.

References

Aris R (1956) On the dispersion of a solute in a fluid flowing through a tube. Proc R Soc Lond A 235:67–77

Arulanandam S, Li D (2000) Determining ζ potential and surface conductance by monitoring the current in electro-osmotic flow. J Colloid Interface Sci 225:421–428

Borukhov I, Andelman D (1997) Steric effects in electrolytes: a modified Poisson-Boltzmann equation. Phys Rev Lett 79:435–438

Brotherton CM, Davis RH (2004) Electroosmotic flow in channels with step changes in zeta potential and cross section. J Colloid Interface Sci 270:242–246

Chien RL, Bousse L (2002) Electroosmotic pumping in microchips with nonhomogeneous distribution of electrolytes. Electrophoresis 23:1862–1869

Chien RL, Burgi DS (1992) Sample stacking of an extremely large injection volume in high-performance capillary electrophoresis. Anal Chem 64:1046–1050

Das S, Chakraborty S (2010) Effect of conductivity variations within the electric double layer on the streaming potential estimation in narrow fluidic confinements. Langmuir. doi:10.1021/la1009237

Deen WM (1998) Analysis of transport phenomena. Oxford University Press, New York

Devasenathipathy S, Bharadwaj R, Santiago JG (2007) Investigation of internal pressure gradients generated in electrokinetic flows with axial conductivity gradients. Exp Fluids 43:959–967

Dukhin SS, Derjaguin BV (1974) Surface and colloid science. Wiley, New York

Ghosal S (2002) Lubrication theory for electro-osmotic flow in a microfluidic channel of slowly varying cross-section and wall charge. J Fluid Mech 459:103–128

Herr AE, Molho JI, Santiago JG, Mungal MG, Kenny TW (2000) Electroosmotic capillary flow with nonuniform zeta potential. Anal Chem 72:1053–1057

Huang X, Gordon MJ, Zare RN (1988) Current-monitoring method for measuring the electroosmotic flow rate in capillary zone electrophoresis. Anal Chem 60:1837–1838

Hunter RJ (1992) Foundations of colloid science. Oxford University Press, London

Kirby BJ, Hasselbrink EF Jr (2004) Zeta potential of microfluidic substrates: 1. Theory, experimental techniques, and effects on separations. Electrophoresis 25:187–202

Kjellander R (2009) Intricate coupling between ion-ion and ion-surface correlations in double layers as illustrated by charge inversion-combined effects of strong Coulomb correlations and excluded volume. J Phys 21:424101

Kuo AT, Chang CH, Wei HH (2008) Transient currents in electrolyte displacement by asymmetric electro-osmosis and determination of surface zeta potentials of composite microchannels. Appl Phys Lett 92:244102

Lyklema J (1995) Fundamentals of interface and colloid science. Academic Press, London

Probstein RF (1994) Physicochemical hydrodynamics: an introduction. Wiley, New York

Pu Q, Yun J, Temkin H, Liu S (2004) Ion-enrichment and ion-depletion effect of nanochannel structures. Nano Lett 4:1099–1103

Ren L, Escobedo C, Li D (2001) Electroosmotic flow in a microcapillary with one solution displacing another solution. J Colloid Interface Sci 242:264–271

Ren L, Escobedo C, Li D (2002) A new method of evaluating the average electro-osmotic velocity in microchannels. J Colloid Interface Sci 250:238–242

Ren L, Masliyah J, Li D (2003) Experimental and theoretical study of the displacement process between two electrolyte solutions in a microchannel. J Colloid Interface Sci 257:85–92

Stein D, Kruithof M, Dekker C (2004) Surface-charge-governed ion transport in nanofluidic channels. Phys Rev Lett. 93:035901

Sze A, Erickson D, Ren L, Li D (2003) Zeta-potential measurement using the Smoluchowski equation and the slope of the current-time relationship in electroosmotic flow. J Colloid Interface Sci 261:402–410

Takamura Y, Onoda H, Inokuchi H, Adachi S, Oki A, Horiike Y (2003) Low-voltage electroosmosis pump for stand-alone microfluidics devices. Electrophoresis 24:185–192

Taylor GI (1953) Dispersion of soluble matter in solvent flowing slowly through a tube. Proc R Soc Lond A 219:186–203

Wang C, Wong TN, Yang C, Ooi KT (2007) Characterization of electroosmotic flow in rectangular microchannels. Int J Heat Mass Transf 50:3115–3121

Yossifon G, Chang YC, Chang HC (2009) Rectification, gating voltage, and interchannel communication of nanoslot arrays due to asymmetric entrance space charge polarization. Phys Rev Lett 103:154502